Ceramics International 44 (2018) 3517–3522

Contents lists available at ScienceDirect

Ceramics International

journal homepage: www.elsevier.com/locate/ceramint

Short communication

# Synthesis and structural evolution of partially and fully stabilized $ZrO_2$ from a versatile method aided by microwave power

E. Silva Junior[a,*], S.G. Antonio[a], E. Longo[a,b]

[a] São Paulo State University (Unesp), Institute of Chemistry, Araraquara, São Paulo 14800-060, Brazil
[b] Federal University of São Carlos (UFSCar), Department of Chemistry, São Carlos, São Paulo 13565-905, Brazil

ARTICLE INFO

*Keywords:*
Gadolinium-doped zirconia
Microwave heating
Structural stabilization
Order-disorder degree

ABSTRACT

We propose a simple, fast, and economical method to obtain $ZrO_2$ powders aided by microwave heating. Partially stabilized zirconia (tetragonal + monoclininc) undergoes transition to fully stabilized zirconia in the tetragonal phase as $Gd^{3+}$ ions are incorporated (0.5–5 mol%) into the zirconium precursor solution and posteriorly annealed at 300, 500 and 700 °C for 15 min in an adapted household microwave oven. XRD, Rietveld refinement and Raman scattering results confirm that structural evolution of zirconia occurs due to the presence structural ordering at both long- and short-range, whose fully stabilization, and hence, the higher structural order-disorder degree, was kept only for doping content at 5% of $Gd^{3+}$ by the elimination of secondary phase (monoclinic). TEM/HRTEM/SAED results revealed that partially and fully stabilized $ZrO_2$ are polycrystalline materials composed by an agglomerate of nanoparticles formed due to the fast microwave heating.

## 1. Introduction

The $ZrO_2$ polymorphism is a limiting factor for many its technological applications, mainly, at high temperatures [1–5]. Tetragonal zirconia under elevated temperatures tends to the exhibit a large volume change (3–5%) along cooling process to the monoclinic phase around to 970 °C [1,4]. Therefore, one of the major challenges in the use of $ZrO_2$ lies in the difficulty in to obtain a stable crystalline structure, *i.e.*, fully stabilized zirconia (FSZ) [1], mainly, in the tetragonal and cubic phases which are more valuable for technological applications [6–15]. However, zirconia stabilized can be obtained by the incorporation of stabilizing agents such as divalent cations ($Mg^{2+}$ [16], $Ca^{2+}$ [17]) and/or trivalent rare earth cations ($Y^{3+}$ [12,18,19], $Gd^{3+}$ [20–22], $Eu^{3+}$ [9,23,24], $Er^{3+}$ [8,25] and $Tb^{3+}$ [26,27]. Huang and co-workers [20] reported that addition of $Gd^{3+}$ ions (5–40% mol) reduces the needed reaction temperature or duration for the formation of the $ZrO_2$ nanocrystals as well as the phase selective effect for the formation of cubic $ZrO_2$. Ilanchezhiyan et al. [22] verificated that insertion of 3–5 wt % $Gd^{3+}$ besides to promote the structural stabilization, promoted a blue shift effect in the absorption edge of $ZrO_2$ and an improvement of the dielectric properties of $ZrO_2$ complexes. Tamrakar and Upadhyay [28] observed that for range doping 0.5–3 mol%. of $Gd^{3+}$, only cubic $ZrO_2$ was obtained and the optical performance exhibited an intense UV emission up to 2.5% of $Gd^{3+}$, whereas the red emission decreases with increasing $Gd^{3+}$ concentration. Stabilized zirconia can be obtained by several methods such as sol-gel [29–33], spray pyrolysis [34], co-precipitation [22,35], hydrothermal/solvothermal [8,20,36], electrochemical deposition [37] and combustion [23,26,38]. Nevertheless, most of these methods shows disadvantages related to the employed of high reaction temperatures, expensive processing techniques and long reaction times. Therefore, the main goal of present work was to find a simple and versatile method for preparing partially stabilized zirconia (pristine $ZrO_2$) and fully stabilized zirconia (gadolinium-doped $ZrO_2$) from a combination of the sol-gel process and post annealing, both performed by microwave power.

## 2. Experimental

Pristine and Gd-doped $ZrO_2$ were obtained by a two-step synthetic route, both assisted by microwave heating systems using adapted household microwave ovens (Fig. 1). Thereby, in the first microwave heating system (see Fig. 1a), the zirconium ($ZrO(NO_3)_2.xH_2O$ - 99%, Aldrich) and gadolinium ($Gd(NO_3)_3{\cdot}6H_2O$ - 99%, Aldrich) precursors solutions (sol) were placed into sealed autoclave (Teflon® cup and a manometer). After turning on the microwave power, microwave irradiation cross in Teflon® cup, once this one not absorbing it, increasing the thermal/kinetics effects of the reaction medium to expedite the sol-gel transition (gelation). In the second microwave heating system (see Fig. 1(b)), the xerogels were placed on the alumina crucible and covered by a SiC crucible, which absorber the microwave irradiation for

* Corresponding author.
*E-mail address:* euripedessj@gmail.com (E. Silva Junior).

https://doi.org/10.1016/j.ceramint.2017.11.145
Received 24 July 2017; Received in revised form 19 November 2017; Accepted 20 November 2017
Available online 21 November 2017

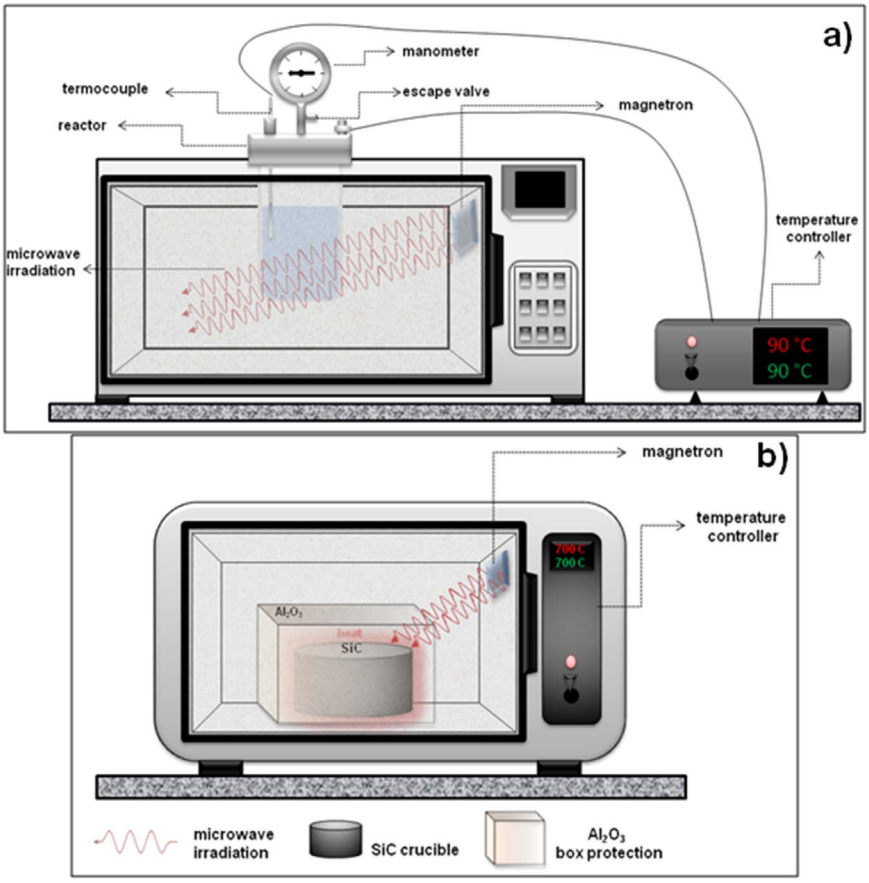


**Fig. 1.** Microwave heating system employed to expedite the sol-gel transition (a). Microwave heating system performed to promote the crystallization of the $ZrO_2$ samples (b).

transformed it in heat to promote the crystallization stage. A box protection of $Al_2O_3$ was placed over SiC crucible to avoid superheating. A thermocouple, not shown in the Fig. 1b, is in contact with alumina crucible to monitor the sample temperature. Details of the procedure to obtaining of the pristine $ZrO_2$ and Gd-doped $ZrO_2$ samples and the characterization techniques can be verificated on the Supplementary Material.

## 3. Results and discussion

Fig. 2 shows the Raman spectra of the pristine and Gd-doped $ZrO_2$ processed at 300, 500 and 700 °C and of the material untreated thermally. As can observed in Fig. 2(a), the pristine $ZrO_2$ sample without microwave annealing (as-prepared $ZrO_2$) no exhibits a typical Raman spectrum for a crystalline $ZrO_2$, *i.e.*, is an amorphous $ZrO_2$. However, in Fig. 2(a), the $ZrO_2$ samples subjected to the microwave annealing at 300 °C, 500 °C and 700 °C, display Raman spectra with vibrational modes characteristic of the $ZrO_2$ crystalline. The $ZrO_2$ sample processed at 300 °C (Fig. 2(a)) presented weak peaks indicating very low degree of crystallinity at short-range. All vibrational modes observed in the Raman spectra (Fig. 2(a-d)) are localized at 147, 178, 190, 267, 223, 317, 333, 346, 381, 475, 502, 539, 562, 618 and 647 $cm^{-1}$. According to group theory [39,40], the Raman-active modes localized at 147 ($E_g$), 267 ($E_g$), 317 ($B_{1\,g}$), 475 ($B_{1\,g}$) and 647 $cm^{-1}$ ($A_{1\,g}$) are associated to the tetragonal phase, while the presence of the monoclinic phase is assigned to Raman-active modes located at 178 $cm^{-1}$ ($A_g$ + $B_g$), 190 ($B_g$), 223 ($A_g$), 333 ($A_g$), 346 ($B_g$), 381 ($B_g$), 475 ($B_g$), 539 ($B_g$), 502 ($A_g$), 539 ($B_g$), 562 ($B_g$) and 618 ($A_g$) $cm^{-1}$ [41,42]. The increasing of dopant concentration into the $ZrO_2$ lattice tends to enhance the structural stabilization, at short-range, in the tetragonal phase (see Fig. 2(c)–(d)). However, with doping concentration of 2.5 mol%, a very weak shoulder close to the band localized at 600 $cm^{-1}$ was detected which is assigned to the monoclinic phase (Fig. 2(c)). Thereby, it is not clear, only with Raman results, that $ZrO_2$ with 2.5 mol% of $Gd^{3+}$ is a fully stabilized zirconia, at short-range, in tetragonal phase. On the other hand, for 5 mol% of $Gd^{3+}$ only the Raman-active modes assigned to the tetragonal phase are observed (see Fig. 2(d)).

From the analysis of the structural ordering at long-range, the XRD pattern (Fig. 3) reveled that when the xerogel is not processed by microwave heating (Fig. 1b), the $ZrO_2$ structure exhibits high structural disorder at long-range, compatible to XRD pattern of amorphous $ZrO_2$, in good according Raman result (Fig. 2a). However, when the xerogels are annealing through microwave heating (Fig. 1b), the Rietveld refinement (TOPAS Academic v. 5.0 [43]) data (Table 1) and the XRD patterns (Fig. 4) shown that crystalline $ZrO_2$ were obtained. The reliability factors, $R_{wp}$ and Gof (goodness-of-fit), shown in Table 1, confirm the good refinement quality [44]. The incorporation of $Gd^{3+}$ ions into the $ZrO_2$ lattice caused a decreasing in the diffraction intensities, so that the degree of crystallinity of the Gd-doped $ZrO_2$ is lower than pristine $ZrO_2$. Despite the microwave annealing to promote the crystallization of the $ZrO_2$ xerogels, the pristine $ZrO_2$ (Fig. 4a-c) and Gd-doped $ZrO_2$ with 0.5 mo % of $Gd^{3+}$ (Fig. 4d) exhibited two crystallographic structures assigned to the tetragonal (ICSD#85322) and monoclinic (ICSD#18190) phases, independent of the processing temperature (see Table 1), *i.e.*, partially stabilized zirconia, at long-range, were obtained. On the other hand, the fully stabilized zirconia, at long-range, in the tetragonal phase (ICSD#85322) were obtained when the $Gd^{3+}$ ions are incorporated into the $ZrO_2$ lattice for doping concentration of 2.5 and 5 mol% (Fig. 4(e, f)). The choice of the Gd doped-$ZrO_2$ samples processed at 300 °C for XRD analysis occurred because the most deviation in the phase content (see Table 1) was observed for these samples. Thereby, the structural stabilization for these samples would be the most difficult to achieve. Rietveld refinement revealed that at doping concentration of 2.5 and 5 mol%, the zirconia is fully

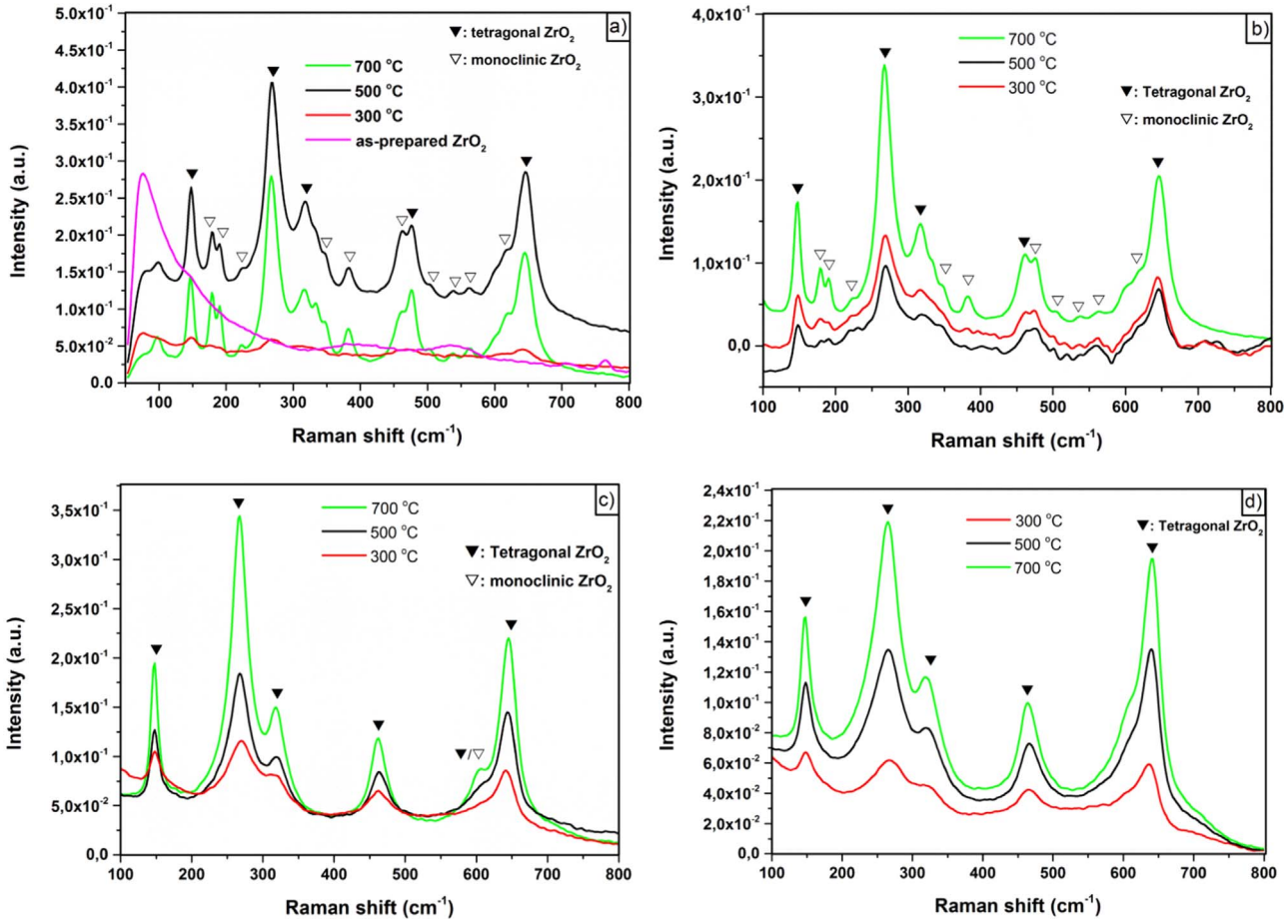


**Fig. 2.** Raman spectra of the as-prepared $ZrO_2$ and pristine $ZrO_2$ obtained by the proposed method in different temperatures of processing (a). Raman spectra of the Gd-doped $ZrO_2$ obtained by the proposed method in different temperatures of processing with $Gd^{3+}$ doping concentration of 0.5 mol%, (b); 2.5 mol% (c); 5 mol% (d).

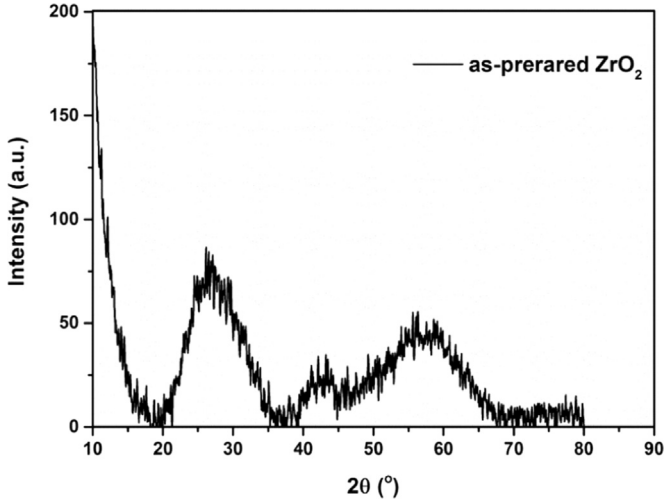


**Fig. 3.** XRD pattern of the pristine $ZrO_2$ obtained without microwave heating (as-prepared $ZrO_2$).

stabilized in the tetragonal phase at long-range, whereas at short-range, Raman results shown that only for 5 mol% the stabilization is obtained. Low valence cations, such as trivalent lanthanide ions, tend to increases the oxygen vacancy concentration to ensure the charge balance of the $ZrO_2$ crystal, which in turn induce extrinsic defects on the $ZrO_2$ lattice such as, internal stress, strain and distortions changing the crystal field surrounding [45–47]. Therefore, the fully stabilized $ZrO_2$ in the tetragonal phase, in according DRX, Rietveld refinement and Raman

**Table 1**
Rietveld refinement parameters of the pristine and Gd-doped $ZrO_2$.

| **Pristine $ZrO_2$** | | | | | | |
|---|---|---|---|---|---|---|
| **Temp.[a] proc.** | 300 °C | | 500 °C | | 700 °C | |
| **$R_{wp}$** | 8.1 | | 8.7 | | 8.0 | |
| **Gof** | 1.7 | | 1.9 | | 1.6 | |
| **phases %** | *t*-$ZrO_2$ | *m*-$ZrO_2$ | *t*-$ZrO_2$ | *m*-$ZrO_2$ | *t*-$ZrO_2$ | *m*-$ZrO_2$ |
| | 68.1 (3) | 31.9(3) | 85.0(2) | 15.0(2) | 77.1(2) | 22.9(2) |
| **Gd-doped $ZrO_2$ (300 °C)** | | | | | | |
| **Doping cont[b]** | 0.5% $Gd^{3+}$ | | 2.5% $Gd^{3+}$ | | 5% $Gd^{3+}$ | |
| **$R_{wp}$** | 6.7 | | 8.7 | | 7.7 | |
| **Gof** | 1.5 | | 1.6 | | 1.6 | |
| **phase %** | *t*-$ZrO_2$ | *m*-$ZrO_2$ | *t*-$ZrO_2$ | *m*-$ZrO_2$ | *t*-$ZrO_2$ | *m*-$ZrO_2$ |
| | 86.4(8) | 13.6(8) | 100 | – | 100 | – |

[a] Temperature of processing.
[b] Doping content (% mol). *t*-$ZrO_2$ = tetragonal. *m*-$ZrO_2$ = monoclinic.

scattering results, can be attributed to the oxygen vacancies generated due to the mismatch ionic radius between $Gd^{3+}$ ($r_{ion}$~1.07 Å) and $Zr^{4+}$ ($r_{ion}$ ~0.86 Å) entailing the substitution of the cations $Zr^{4+}$ by $Gd^{3+}$ [20–22].

The classical sol-gel method usually requires a heat treated in order to obtain a crystalline material at the end of the process [48]. In this sense, Montoya and co-workers [30] prepared by annealing dried gels of $Gd_xZr_{1-x}O_2$ ($0 \leq x \leq 0.2$) at temperatures between 450 and 1.300 °C for 3 h under conventional heating. The authors observed that for low Gd doping content ($x < 0.05$), *t*-$ZrO_2$ were obtained up to 1.100 °C, whereas the *m*-$ZrO_2$ were detected up to 1.300 °C. Behera et al. [31] reported stabilization of the *t*-$ZrO_2$ at concentration range

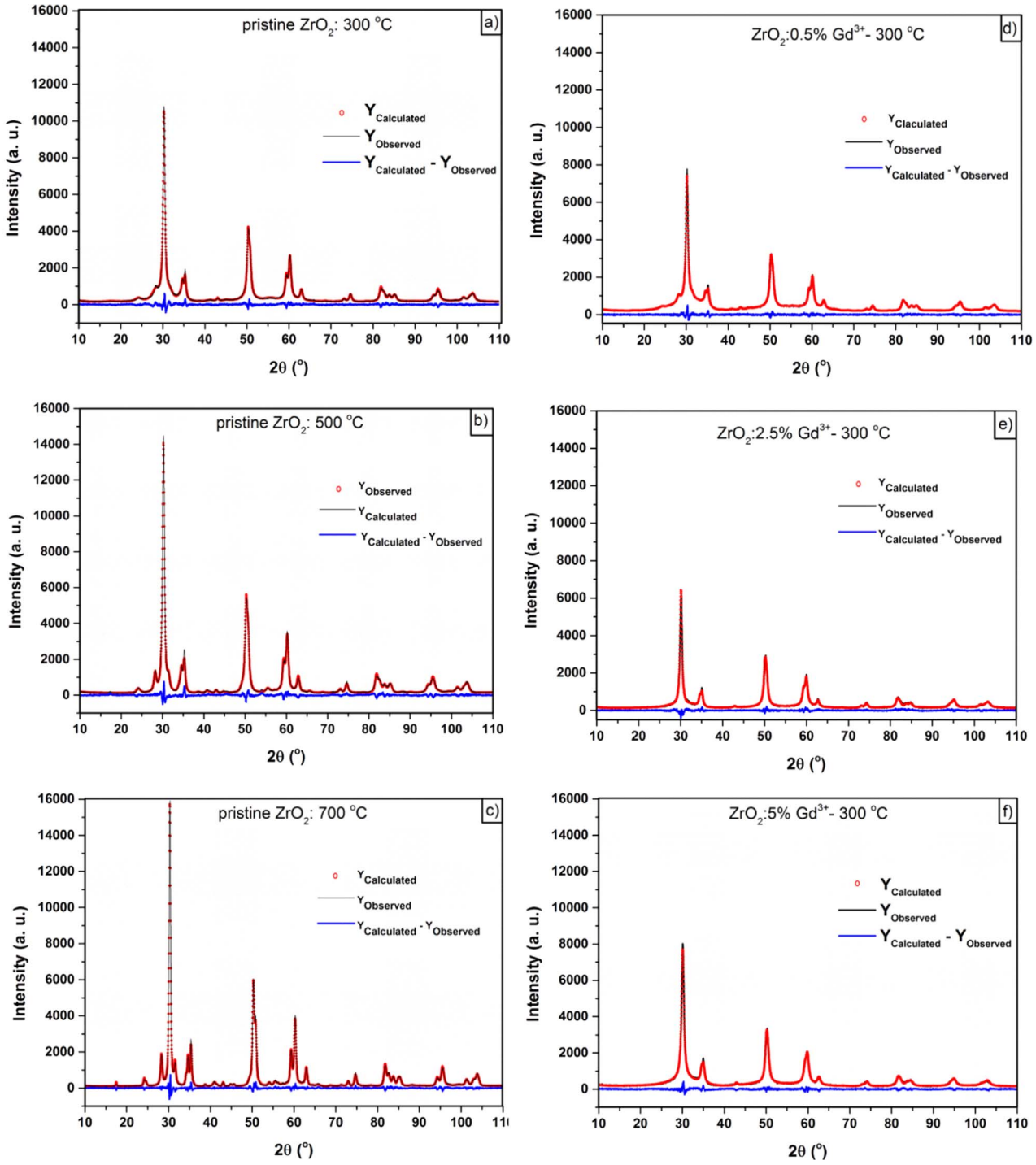


**Fig. 4.** XRD patterns from Rietveld refinements data of the pristine $ZrO_2$ (a-c) and Gd-doped $ZrO_2$ (d-f) obtained from proposed method and processed at 300 °C.

(5–10 mol%) of $Gd^{3+}$ under heat treated at different temperatures (300–1100 °C) for 4 h, whereas higher dopants contents (> 10 mol%) leaded to the formation of cubic $ZrO_2$ (*c*-$ZrO_2$). Manjunatha and Dharmaprakash [33] managed to get FSZ (*c*-$ZrO_2$) by co-doping with 2.5 mol% of $Gd^{3+}$ and 2.5 mol% of $Eu^{3+}$ using a microwave assisted solution combustion method during 30 s of time processing. Therefore, the chemical and structural evolutions taking place in the $ZrO_2$ depend strongly of the type of heat treat employed in the sol-gel process (combustion method, microwave power, conventional heating, *etc.)* as well as of the processing time.

Fig. 5 illustrates TEM/HRTEM/SAED images of the pristine $ZrO_2$ and Gd-doped $ZrO_2$ (5 mol% of $Gd^{3+}$), both processed at 700 °C. TEM (Fig. 5(a, d) and HRTEM images (Fig. 5(b, e)) revealed that $ZrO_2$ particles tend to agglomerate like nanoparticles with heterogeneous size distribution. Thereby, the TEM/HRTEM images implies that the nucleation and growth mechanisms are governed by the coalescence process, whose attachment mechanism occurs randomly between grain boundaries with crystallographic misorientation to form the $ZrO_2$ nanoparticles [49,50]. Fig. 5(c, f) exhibit the SAED patterns with well-defined rings, characteristic of the polycrystalline materials, produced by the diffraction from the various families of planes (*t*-$ZrO_2$ and *m*-$ZrO_2$) within the randomly oriented crystals [51]. For pristine $ZrO_2$ sample (Fig. 5c), the indexing SAED pattern revealed that *t*-$ZrO_2$ was well indexed by the appearance of the characteristic planes T(011),

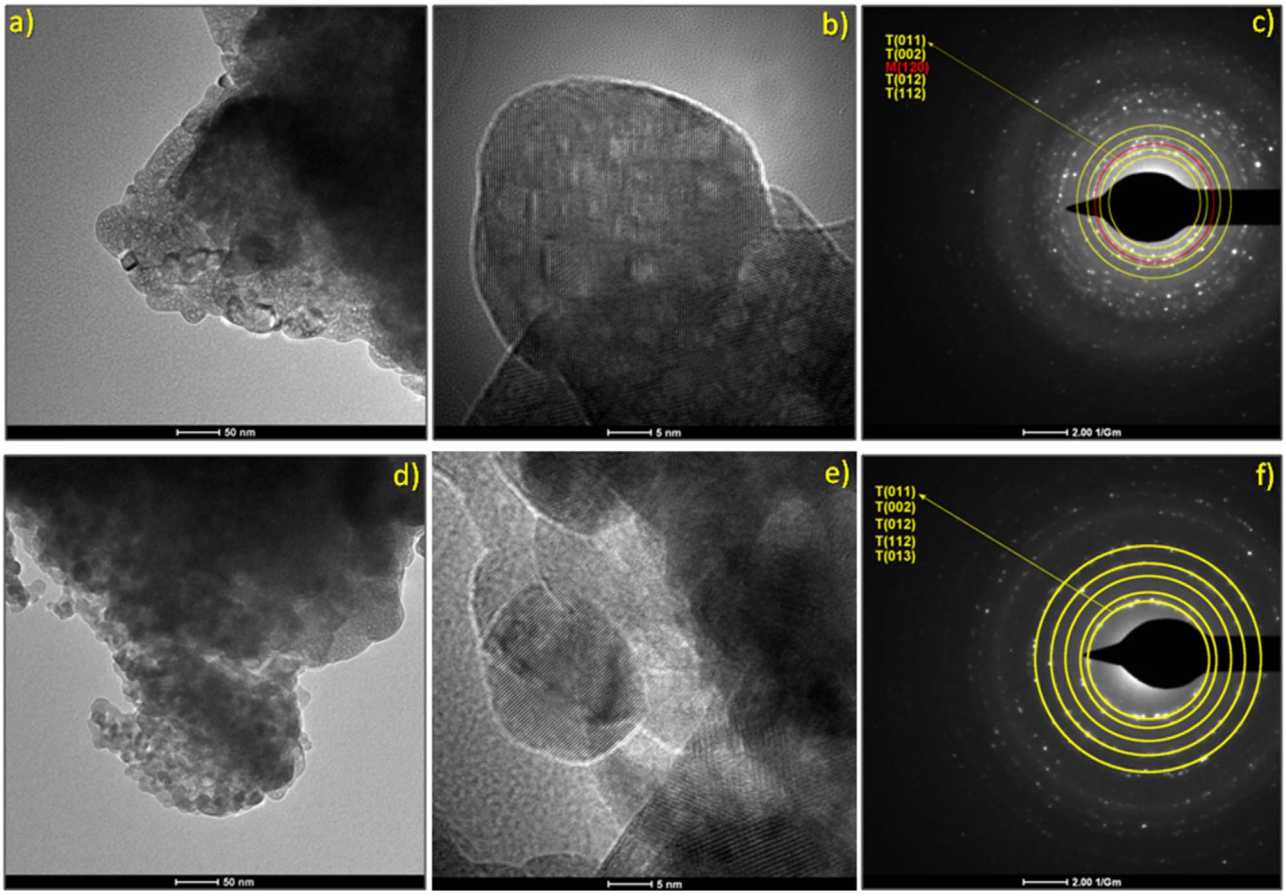


**Fig. 5.** TEM, HRTEM and SAED of the pristine $ZrO_2$ and Gd-doped $ZrO_2$ (5 mol% of $Gd^{3+}$) both processed at 700 °C. Pristine $ZrO_2$ = TEM (a), HRTEM (b) and SAED (c). Gd-doped $ZrO_2$ = TEM (d), HRTEM (e) and SAED (f).

T(002), T(012), T(112) and T(013). However, the plane M(120), ascribed to the *m*-$ZrO_2$, also was indexed. On the other hand, the SAED pattern (Fig. 5f) shown that for doping concentration at 5 mol% of $Gd^{3+}$ FSZ (*t*-$ZrO_2$) was obtained, once only the planes T(011), T(002), T(012), T(112) and T(013), ascribed to the *t*-$ZrO_2$ were well indexed.

## 4. Conclusion

Partially and fully stabilized zirconia powders were successfully synthesized from route aided by microwave power, using simpler and faster processing steps as compared to the conventional methods reported in literature. The microwave heating mechanism provided a particular energy transfer which promoted a fast crystallization of the $ZrO_2$ samples, besides to antecede the gel point. The FSZ can be attributed to the oxygen vacancies created entailing the enough substitution of $Zr^{4+}$ by $Gd^{3+}$ ions (5 mol%) which induce extrinsic defects on the $ZrO_2$ lattice such as, internal stress, strain and distortions thereby stabilizes in the tetragonal phase. Therefore, considering its viability, the method proposed here showed to be a very promising to obtain rare-earth doped zirconia powders highly stabilized, at both long- and short-range.

## Acknowledgements

This work was supported by the Brazilian research agencies: CNPq (Project: 402923/2014-6; Process: 157575/2015-2) and FAPESP-CEPID/CDMF 2013/07296-2.

## Appendix A. Supplementary material

Supplementary data associated with this article can be found in the online version at http://dx.doi.org/10.1016/j.ceramint.2017.11.145.

## References

[1] O. Ohtaka, H. Fukui, T. Kunisada, T. Fujisawa, K. Funakoshi, W. Utsumi, T. Irifune, K. Kuroda, T. Kikegawa, Phase relations and equations of state of $ZrO_2$ under high temperature and high pressure, Phys. Rev. B 63 (2001) 174108–174115.
[2] A. Hirvonen, R. Nowak, Y. Yamamoto, T. Sekino, K. Niihara, Fabrication, structure, mechanical and thermal properties of zirconia-based ceramic nanocomposites, J. Eur. Cer. Soc. 26 (2006) 1497–1505.
[3] A.R. Studart, U.T. Gonzenbach, E. Tervoort, L.J. Gauckler, Processing routes to macroporous ceramics: a review, J. Am. Ceram. Soc. 89 (2006) 1771–1789.
[4] R.A. Rocha, E.N.S. Muccillo, L. Dessemond, E. Djurado, Thermal ageing of nanostructured tetragonal zirconia ceramics: characterization of interfaces, J. Eur. Cer. Soc. 30 (2010) 227–231.
[5] N.J. Lóh, L. Simão, C.A. Faller, A. De Noni, O.R.K. Montedo, A review of two-step sintering for ceramics, Ceram. Int. 15 (2016) 12556–12572.
[6] L.K. Dash, N. Vast, P. Baranek, M. –C. Cheynet, L. Reining, Electronic structure and electron energy-loss spectroscopy of $ZrO_2$ zirconia, Phys. Rev. B: Condens. Matter Mater. Phys. 70 (2004) 245116–245132.
[7] J.C. Ray, D.-W. Park, W.-S. Ahn, Chemical synthesis of stabilized nanocrystalline zirconia powders, J. Ind. Eng. Chem. 12 (2006) 142–148.
[8] B.J. Lopez, V.D.L. Luz, F. Gonell, E. Cordonicillo, M.L. Haro, J.J. Calvino, P. Escribano, Key insights on the structural characterization of textured $Er_2O_3$–$ZrO_2$ nano-oxides prepared by a surfactant-free solvothermal route, J. Alloy. Compd. 519 (2012) 29–36.
[9] S.D. Meetei, Sh.D. Singh, V. Sudarshan, Polyol synthesis and characterizations of cubic $ZrO_2$:$Eu^{3+}$ nanocrystals, J. Alloy. Compd. 514 (2012) 174–178.
[10] Y. Tanaka, T. Sato, H. Ikeda, N. Miura, Cobalt-based solid reference-electrode usable in zirconia-based sensors for detection of oxygen or volatile organic compounds, Sens. Actuat. B: Chem. 203 (2014) 899–903.
[11] E. Moretti, L. Storaro, A. Talon, S. Chitsazan, G. Garbarino, G. Busca, E. Finocchio, Ceria-zirconia based catalysts for ethanol steam reforming, Fuel 153 (2015) 166–175.

[12] S. Nath, I. Manna, J.D. Majumdar, Nanomechanical behavior of yttria stabilized zirconia (YSZ) based thermal barrier coating, Ceram. Int. 41 (2015) 5247–5256.
[13] V. Pouchly, K. Maca, Sintering kinetic window for yttria-stabilized cubic zirconia, J. Eur. Ceram. Soc. 36 (2016) 2931–2936.
[14] R.E. Soltis, M.P. McQuillen, G. Surnilla, Blackening in Zirconia-based electrochemical oxygen sensor at high pumping potentials, ECS Trans. 75 (2016) 73–82.
[15] S. Il Lee, M. Park, J. Hong, H. Kim, J.-W. Son, J.-H. Lee, B.-K. Kim, H.-W. Lee, K.J. Yoon, Fabrication of dense and defect-free diffusion barrier layer via constrained sintering for solid oxide fuel cells, J. Eur. Cer. Soc. 37 (2017) 3219–3223.
[16] L.R. Renuka, K.S. Anantharaju, S.C. Sharma, H.P. Nagaswarupa, S.C. Prashantha, H. Nagabhushana, Y.S. Vidya, Hollow microspheres Mg-doped $ZrO_2$ nanoparticles: green assisted synthesis and applications in photocatalysis and photoluminescence, J. All. Comp. 672 (2016) 609–622.
[17] C.H. Lin, X.F. Zhang, Y. Hou, Y.L. Wang, G. Wang, Synthesis of calcium oxide stabilized cubic zirconia powders by electrochemical method, Adv. Mat. Res. 233–235 (2011) 2403–2408.
[18] V.F. Petrunin, S.A. Korovin, Preparation of nanocrystalline powders of $ZrO_2$, stabilized by $Y_2O_3$ dobs for ceramics, Phys. Proc. M 72 (2015) 544–547.
[19] V. Pouchly, K. Maca, Sintering kinetic window for yttria-stabilized cubic zirconia, J. Eur. Ceram. Soc. 36 (2016) 2931–2936.
[20] F. Huang, D. Chen, J. Zhou, Y. Wang, Modifying the phase and controlling the size of monodisperse $ZrO_2$ nanocrystals by employing $Gd^{3+}$ as a nucleation agent, Cryst. Eng. Commun. 13 (2011) 4500–4502.
[21] R.K. Tamrakar, K. Upadhyay, Combustion synthesized $ZrO_2$ $Gd^{3+}$ nanophosphors: structural and photoluminescence studies, J. Mater. Sci: Mater. Electron 28 (2017) 12545–12550.
[22] P. Ilanchezhiyan, C. Siva, T.W. Kang, G.M. Kumar, Colloidal synthesis of $Gd^{3+}$ doped $ZrO_2$ based dielectrics and their structural and electrochemical property studies, J. Mater. Sci: Mater. Electron 27 (2016) 5557–5562.
[23] Y.S. Vidya, K.S. Anantharaju, H. Nagabhushana, S.C. Sharma, H.P. Nagaswarupa, S.C. Prashantha, C. Shivakumara, Danithkumar, Combustion synthesized tetragonal $ZrO_2$:$Eu^{3+}$ nanophosphors: structural and photoluminescence studies, Spectrochim. Acta A Mol. Biomol. Spectrosc. 135 (2015) 241–251.
[24] Y. Hui, Y. Zhao, S. Zhao, L. Gu, X. Fan, L. Zhu, B. Zou, Y. Wanga, X. Cao, Fluorescence of $Eu^{3+}$ as a probe of phase transformation of zirconia, J. All. Comp. 573 (2013) 177–181.
[25] M.R.N. Soares, T. Holz, F. Oliveira, F.M. Costa, T. Monteiro, Tunable green to red $ZrO_2$:Er nanophosphors, Mater. Sci. Eng. B. 177 (2012) 712–716.
[26] S. López-Romero, M. García-Hipólito, A. Aguilar-Castillo, Bright green luminescence from zirconium oxide stabilized with $Tb^{3+}$ ions synthesized by solution combustion technique, W. J. Cond. Mat. Phys. 3 (2013) 173–179.
[27] S. Yatsunenko, J. Kaszewski, J. Grzyb, I. Pełech, M.M. Godlewski, E. Mijowska, U. Narkiewicz, M. Godlewski, Impact of yttria stabilization on $Tb^{3+}$ intra-shell luminescence efficiency in zirconium dioxide nanopowders, J. Phys. Condens. Matter 25 (2013) (15 194106/1-6).
[28] R.K. Tamrakar, K. Upadhyay, Combustion synthesized $ZrO_2$ $Gd^{3+}$ nanophosphors: structural and photoluminescence studies, J. Mater. Sci: Mater. Electron. 28 (2017) 12545–12550.
[29] Y. Chang, C. Wang, T. Liang, C. Zhao, X. Luo, T. Guo, J. Gong, H. Wu, Sol–gel synthesis of mesoporous spherical zirconia, RSC Adv. 5 (2015) 104629–104634.
[30] N. Montoya, P. Pardo, A. Doménech-Carbó, J. Alarcón, Structural stability and electrochemical properties of Gd-doped $ZrO_2$ nanoparticles prepared by sol–gel, J. Sol.-Gel Sci. Technol. 69 (2014) 137–147.
[31] P.S. Behera, S. Vasanthavel, V. Ponnilavan, S. Kannan, Influence of gadolinium content on the tetragonal to cubic phase transition in zirconia-silica binary oxides, J. Sol. Sta. Chem. 225 (2015) 305–309.
[32] H.S. Lim, A. Ahmad, H. Hamazah, Synthesis of zirconium oxide nanoparticle by sol-gel technique, AIP Conf. Proc. 1571 (2013) 812–816.
[33] S. Manjunatha, M.S. Dharmaprakash, Eu + 3 Ion as a Luminescent Probe in $ZrO_2$: $Gd^{+3}$ co-doped nanophosphor, Int. J. Innov. Res. Sci. Eng. Technol. 11 (2017) 56–59.
[34] S.B. Deshmukh, R.H. Bari, Nanostructured $ZrO_2$ thin films deposited by spray pyrolysis techniques for ammonia gas sensing application, Int. Lett. Chem. Phys. Astron. 56 (2015) 120–130.
[35] L.X. Lovisa, J. Andres, L. Gracia, M.S. Li, C.A. Paskocimas, M.R.D. Bomio, V.D. Araujo, E. Longo, F.V. Motta, Photoluminescent properties of $ZrO_2$:$Tm^{3+}$, $Tb^{3+}$, $Eu^{3+}$ powders: a combined experimental and theoretical study, J. All. Comp. 695 (2017) 3094–3103.
[36] A. Behbahani, S. Rowshanzamir, A. Esmaeilifar, Hydrothermal synthesis of zirconia nanoparticles from commercial zirconia, Proc. Eng. 42 (2012) 908–917.
[37] V.S. Protsenko, E.A. Vasil'eva, I.V. Smenova, A.S. Baskevich, I.A. Danilenko, T.E. Konstantinov, F.I. Danilov, Electrodeposition of Fe and Composite Fe/$ZrO_2$ Coatings from a Methanesulfonate Bath, Sur. Eng. Appl. Electrochem. 51 (2015) 65–75.
[38] B. Marían, K.C. Singh, M. Sahal, S.P. Khatkar, V.B. Taxak, M. Kumar, Preparation and luminescence properties of $Tb^{3+}$ doped $ZrO_2$ and $BaZrO_3$ phosphors, J. Lumines 130 (2010) 2128–2132.
[39] E. Anastassakis, B. Papanicolaou, I.M. Asher, Lattice dynamics and light scattering in hafnia and zirconia, J. Phys. Chem. Solids 36 (1975) 667–676.
[40] C.M. Phillippi, K.S. Mazdiyasni, Infrared and raman spectra of zirconia polymorphs, J. Am. Ceram. Soc. 54 (1971) 254–258.
[41] A.P. Naumenko, N. Berezovska, M.M. Billy, O.V. Schevchenko, Vibrational analysis and Raman spectra of tetragonal Zirconia, Phys. Chem. Solid Stat. 9 (2008) 121–125.
[42] F. Davara, M.R. Loghman-Estarki, Synthesis and optical properties of pure monoclinic zirconia nanosheets by a new precursor, Ceram. Int. 40 (2014) 8427–8433.
[43] A. Coelho, Coelho Sofware: topas Academic v. 5.0, Topas Academic, Brisbane (2007).
[44] H.M. Rietveld, A profile refinement method for nuclear and magnetic structures, Acta Cryst. 2 (1969) 65–71.
[45] S. Fabirs, A.T. Paxton, M.W. Finnis, A stabilization mechanism of zirconia based on oxygen vacancies only, Acta Mater. 50 (2002) 5171–5178.
[46] Y. Xie, Z. Ma, L. Liu, Y. Su, H. Zhao, Y. Liu, Z. Zhang, H. Duan, J. Li, E. Xie, Oxygen defects-modulated green photoluminescence of Tb-doped $ZrO_2$ nanofibers, Appl. Phys. Lett. 97 (2010) (141916/1-3).
[47] J. Tao, An Dong, J. Wang, The influence of microstructure and grain boundary on the electrical properties of scandia stabilized zirconia, Mater. Trans. 54 (2013) 825–832.
[48] J. Livage, C. Sanchez, Sol-gel chemistry, J. Non-Crys. Solid. 145 (1992) 11–19.
[49] H. Zhang, J.J. De Yoreo, J.F. Banfield, A unified description of attachment-based crystal growth, ACS Nano 8 (2014) 6526–6530.
[50] H.Z. Zhang, J.F. Banfield, Energy calculations predict nanoparticle attachment orientations and asymmetric crystal formation, J. Phys. Chem. Lett. 3 (2012) 2882–2886.
[51] J. Lian, J. Zhang, F. Namavar, Y. Zhang, F. Lu, H. Haider, K. Garvin, W.J. Weber, R.C. Ewing, Ion beam-induced amorphous-to-tetragonal phase transformation and grain growth of nanocrystalline zirconia, Nanotechnology 20 (2009) (245303/1-7).